Gas flows around two young stellar clusters in NGC2264

Jonathan P. Williams and Catherine A. Garland

Astronomy Department, University of Florida, Gainesville, FL 32611

ABSTRACT

Observations of the dust and gas toward two young stellar clusters, IRS1 and IRS2, in the NGC2264 star forming region are presented. Continuum emission is used to locate the dusty envelopes around the clusters and individual protostars within and line emission from the $J = 3-2$ transitions of HCO^+ and $H^{13}CO^+$ is used to diagnose the gas flows around them. The molecular abundance, velocity centroid and dispersion are approximately constant across the IRS1 clump. With these constraints, the self-absorbed HCO^+ lines are modeled as a large scale collapse, with speed $v_{in} = 0.3$ km s^{-1} and mass infall rate $\dot{M} = 4 \times 10^{-4}$ $M_\odot$ yr^{-1}, falling onto an expanding central core. The signature of large scale collapse, with a similar speed and mass infall rate, is also found toward IRS2 but again appears disrupted at small scales. Individual protostars are resolved in this cluster and their size and velocity dispersion show that the stellar system is currently bound and no older than 5×10^5 yr, but is destined to become unbound and disperse as the surrounding cloud material is lost.

Subject headings: ISM: individual(NGC2264) — ISM: kinematics and dynamics — stars: formation

1. Introduction

The mass of the molecular ISM is dominated by the largest clouds which tend to form stars in groups, rather than in isolation (Lada et al. 1994). Star formation is inefficient, however, and as the binding mass of a molecular cloud is lost through the action of stellar winds, radiation, and outflows, most groups evaporate (Adams 2000) and become isolated stellar systems. Thus an increased understanding of clustered star formation is essential for learning about the origin of most Galactic disk stars, perhaps including the Sun.

In this paper, we present millimeter wavelength observations of two star formation sites, IRS1 and IRS2, in the NGC2264 region of northern Monoceros. Lying at a distance of 760 pc (Sung, Bessell, & Lee 1997), this region is associated with a moderate mass cloud, $M \simeq 3 \times 10^4$ $M_\odot$ (Oliver, Masheder & Thaddeus 1996), that contains 30 IRAS sources, most classified as Class I protostars (Margulis, Lada, & Young 1989), and ~ 360 near-infrared sources (Lada et al. 1993).

IRS1, also known as Allen's source (Allen 1972), is an early B star situated just north of the Cone nebula. Thompson et al. (1998) postulate that it has triggered the formation of several low mass stars around it and Ward-Thompson et al. (2000) map a number of nearby massive dust condensations suggesting that high mass star formation may also be occuring. Molecular spectral lines show signatures of both outflow (Margulis, Lada, & Snell 1988; Schreyer et al. 1997) and infall (Wolf-Chase & Gregersen 1997; Williams & Myers 1999).

IRS2, discovered by Sargent et al. (1984), is a less luminous and less well studied source $\sim 6'$ to the north of IRS1. A small cluster and nebulosity is visible in the I band image of Lada et al. (1993). Margulis,

Lada, & Snell (1988) found a CO outflow toward this source, Wolf-Chase, Walker, & Lada (1995) mapped an associated dense molecular clump (which they called MonOB1-D), and Williams & Myers (1999) found preliminary evidence for collapse.

Here, we combine continuum observations of the dusty envelopes around the most embedded protostars with spectral line observations of the gas in these two cluster forming regions. The molecular envelopes around the two clusters have a similar mass but are morphologically distinct and present an interesting comparative study. In both cases, the self-absorbed HCO^+ line is used to diagnose relative motions and show large scale collapse onto each stellar group that appears to be disrupted by protostellar outflows on smaller scales. In the bright, compact IRS1 clump, the optically thin $H^{13}CO^+$ line is used to map the molecular abundance, velocity centroid, and dispersion and thereby constrain the modeling of the HCO^+ profiles. In IRS2, where individual protostars are resolved, the size and velocity dispersion is used to estimate an upper limit for their formation time and to determine the gravitational stability of the group. The observations are described in §2, and their analysis in §3. We conclude in §4.

2. Observations

The observations were carried out at the Heinrich Hertz Telescope[1] on Mt. Graham, AZ over a four day period in April 2001. We used the facility 19 channel bolometer to observe continuum emission at 870 μm and the 230 GHz receiver to observe the $J = 3 - 2$ lines of HCO^+ and $H^{13}CO^+$. The weather was good during the run and the zenith opacity at 870 μm ranged from 0.3 to 0.55; for the spectral line observations system temperatures ranged from 350 to 450 K.

The bolometer observations were carried out in dual-beam raster mode with an azimuth scanning velocity of $8''$/sec and a wobbler frequency of 2 Hz. Individual maps had sizes $\sim 8' \times 6'$, sampled at $10''$ in azimuth and elevation, and took 40 minutes to complete. Skydips were made before and after each map to determine the sky opacity and observations of Jupiter and Uranus were used to calibrate the data. Two maps were made of each source at different hour angles and therefore different scan directions across the source. The data were reduced and co-added using the NIC software package resulting in an rms noise in the final maps of 0.14 Jy per $21''$ beam.

The spectral line data were also taken in on-the-fly mode. Maps were made by scanning alternately in right ascension and declination at $3''$/sec with the reference $12'$ west of the map center. Individual map sizes were $\sim 3' \times 2'$, sampled at $10''$, and took ~ 25 minutes each. System temperatures varied from 350 K to 425 K. Maps were repeated several times and made at different offsets, then co-added and stitched together in the CLASS software package so as to achieve an rms noise temperature of 0.8 K (HCO^+) and 0.4 K ($H^{13}CO^+$) per 250 kHz ($\simeq 0.28$ km s^{-1}) channel. The temperature scale was calibrated through the chopper wheel method (Rohlfs & Wilson 1996), and we then applied main beam and forward efficiencies $\eta_{mb} = 0.46$, $\eta_{fss} = 0.92$. Observations of the standard source Orion IRc2 were made daily as an overall check of calibration, pointing, and setup. For both the bolometer and line observations, pointing was checked through observations of Jupiter every 2–3 hours.

---

[1]the Heinrich Hertz Telescope is operated by the Submillimeter Telescope Observatory on behalf of Steward Observatory and the Max-Planck-Institut fuer Radioastronomie.

3. Results

3.1. Bolometer data

The 870 μm continuum emission toward IRS1 and IRS2 is shown in Figure 1. IRS1 is the bright, compact source to the south. Its elongated shape shows signs of substructure; Ward-Thompson et al. (2000) resolve five distinct condensations with higher resolution IRAM and JCMT observations. IRS2 lies to the north and is more fragmented with several low intensity peaks, suggestive of a slightly more evolved cluster in which the individual protostars are beginning to shed their circumstellar envelopes and migrate away from their birthplace.

The integrated fluxes, for flux densities greater than 0.5 Jy beam^{-1}, of the two clusters are similar, 94 Jy for IRS1 (consistent with Ward-Thompson et al.) and 84 Jy for IRS2 indicating that they have similar dust masses and make a good comparative study. The fluxes convert to masses through

$$M = \frac{F_\nu d^2}{\kappa B_\nu(T_d)} = 8.4 \left(\frac{F_\nu}{\mathrm{Jy}}\right) \; M_\odot$$

where we have taken the mass opacity $\kappa = 0.009$ cm^2 g^{-1}, dust temperature $T_d = 17$ K, as in Ward-Thompson et al. (2000) and distance $d = 760$ pc. Thus the total interstellar mass around IRS1 is 790 $M_\odot$ and 710 $M_\odot$ around IRS2. From the projected area of each group, 0.45 pc^2 for IRS1 and 0.62 pc^2 for IRS2, we estimate average column and volume densities $\langle N_{\mathrm{H}_2}\rangle = 8 \times 10^{22}$ cm^{-2}, $\langle n_{\mathrm{H}_2}\rangle = 5 \times 10^4$ cm^{-3} for IRS1 and $\langle N_{\mathrm{H}_2}\rangle = 5 \times 10^{22}$ cm^{-2}, $\langle n_{\mathrm{H}_2}\rangle = 3 \times 10^4$ cm^{-3} for IRS2.

3.2. Line data

The average density of the material traced by the continuum observations is similar to that of HCO$^+$ emitting gas. Indeed, the morphology of the integrated line emission follows the dust (see Figure 2) and we therefore use the line data to investigate the dynamics of the circumcluster material.

The optically thick HCO$^+$ spectra provide information on relative motions, i.e. infall and outflow, in the gas (e.g., Walker et al. (1986)) and the optically thin H^{13}CO$^+$ show the intensity weighted mean velocity and linewidth along each line of sight. We also use the latter to measure the molecular abundance in the IRS1 clump.

The individual protostars in the compact IRS1 clump merge together in the 29″ beam of the line observations and we examine average, group properties. Objects in the more extended IRS2 clump are resolved, however, and we can determine mass infall rates onto both the cluster and a single protostar. In addition, by comparing the cluster's size and velocity dispersion, we estimate its age.

3.2.1. IRS1

Line and continuum data in IRS1 are compared in Figure 2. The left panel overlays contours of integrated H^{13}CO$^+$ intensity over a grayscale of the dust emission. Their similar appearance demonstrates that we can use the line data to examine motions of the circumcluster material. The right panel plots the two quantities on a point by point basis and shows an approximately linear trend over a decade in scale with the implication that the H^{13}CO$^+$ is both optically thin and its abundance constant across the clump. By converting each quantity
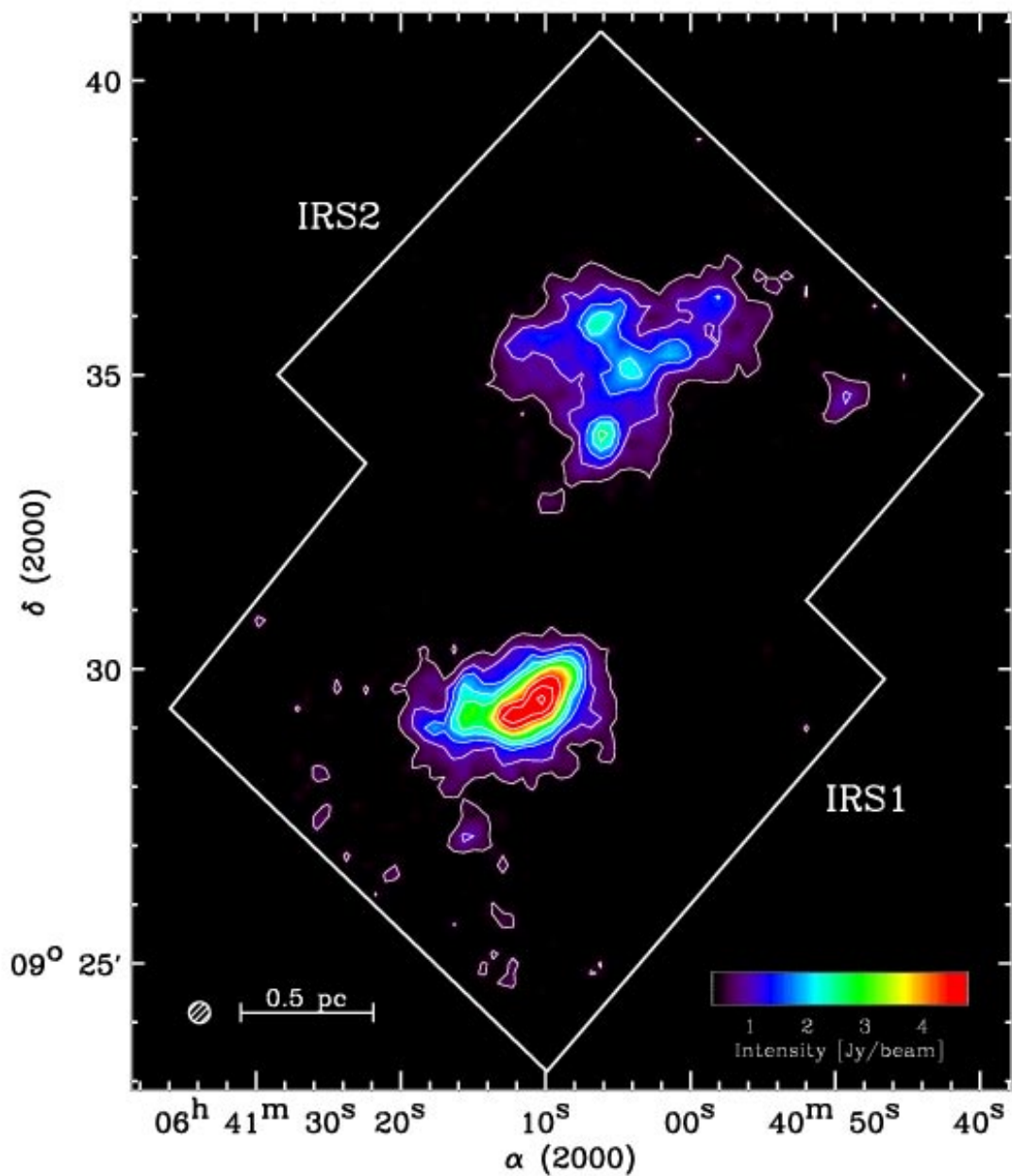
Fig. 1.— 870 μm continuum emission toward IRS1 and IRS2. Black contours are at 0.5, 1.0, 1.5, 2.0, 2.5 Jy beam^{-1}, and white contours are at 3.5, 4.5, 5.5, 6.5 Jy beam^{-1}. The boundary of the map is marked by the heavy solid line and the 21″ beam size is indicated in the lower left corner.

to a column density (assuming an excitation temperature of 20 K for the gas and dust temperature of 17 K) the best fit $H^{13}CO^+$ abundance relative to H_2 is found to be $x(H^{13}CO^+) = 2.0 \times 10^{-11}$. For an isotopic ratio, $^{12}C/^{13}C = 50-100$, the implied HCO^+ abundance lies in the range, $x(HCO^+) = 1-2 \times 10^{-9}$, similar to values in other OB star forming regions (Bergin et al. 1997; Ungerechts et al. 1997). The lack of variation across the clump is demonstrated by the two dashed lines bracketing the data at $x(H^{13}CO^+) = [1.0, 4.0] \times 10^{-11}$.
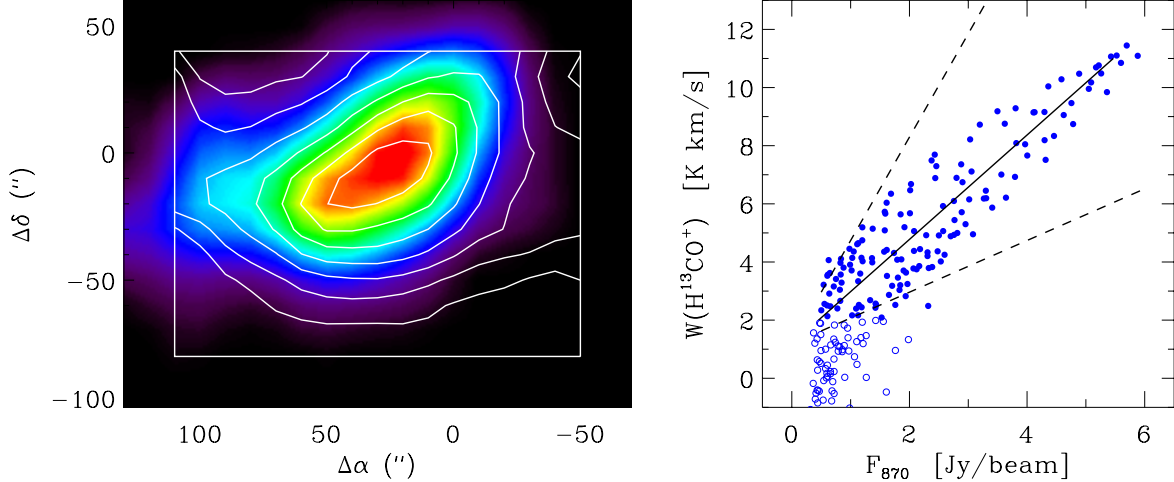

Fig. 2.— Comparison of line and continuum data in the IRS1 clump. The left panel shows contours of $H^{13}CO^+$ emission, integrated over the range $v = 6$ to 10 km s^{-1}, overlayed on a grayscale of the 870 μ thermal continuum emission, smoothed to the $29''$ resolution of the line data. Contours begin and are at intervals of 1.5 K km s^{-1}, and the grayscale ranges from 0.6 to 6.0 Jy beam^{-1}. The close correspondence between the two is shown on a point by point basis in the right panel which plots the integrated $H^{13}CO^+$ intensity versus 870 μ emission. The linear correlation indicates that the $H^{13}CO^+$ emission is optically thin and its abundance constant across the clump. The solid line is a linear least squares fit to the filled circles, $W(H^{13}CO^+) > 2$ K km s^{-1}, and implies an abundance $x(H^{13}CO^+) = 2.0 \times 10^{-11}$ relative to H_2. The dashed lines show abundances factors of 2 lower and higher.

Higher moments of the $H^{13}CO^+$ emission show the variation of mean velocity and dispersion across the cluster (Figure 3) The former increases from 7.0 km s^{-1} toward the East to 8.4 km s^{-1} at center, but then returns to a lower value, ~ 7.8 km s^{-1} in the West. There is no clearly defined rotation across the clump and toward the central region, $\Delta\alpha = -10''$ to $50''$, the velocity difference, ~ 0.3 km s^{-1}, is much less than the dispersion. The dispersion map itself also shows little variation in this central region and has an average value, $\sigma = 1.0$ km s^{-1}.

The HCO^+ spectra are self-absorbed across the clump: they generally show two peaks and a central dip at the mean velocity of $H^{13}CO^+$. Changes in the velocity of the absorbing gas relative to the emitting gas alter the observed profile and are a diagnostic of relative motions in the clump (Leung & Brown 1977). The relatively poor resolution of the line data, $29'' \simeq 0.1$ pc, does not permit a detailed analysis of the dynamics around individual protostars within this cluster and we therefore focus on global properties, as illustrated in Figure 4. Here, average spectra are shown, computed over different regions of the clump corresponding to different 870 μm flux densities. This is similar to radial averaging but takes into account the non-circular shape of the clump. At low flux densities, corresponding to the outer regions, the average spectra are relatively weak and the optical depths are low. Nevertheless, the HCO^+ spectra are clearly asymmetric and
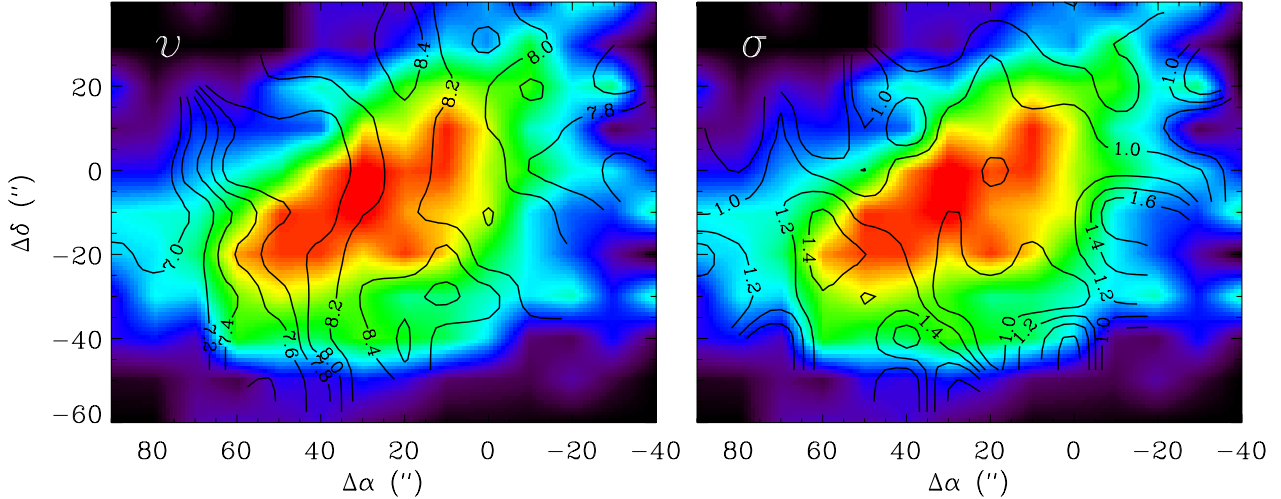
Fig. 3.— Labeled contours of the mean velocity (left panel) and velocity dispersion (right panel) of $H^{13}CO^+$ in the IRS1 core, overlayed on a grayscale of integrated $H^{13}CO^+$ emission. In the central region of the clump, $\Delta\alpha = -10''$ to $50''$, the velocity and dispersion are both approximately constant.

show the red-shifted self-absorption characteristic of inward motions (Walker et al. 1986). At higher flux densities, toward the clump center, the line intensities and optical depths increase and the HCO^+ profiles show two peaks with a central dip. However, the spectra become more symmetric with increasing flux density until at the highest values at the clump's center, the two HCO^+ peaks are of similar intensity suggesting zero average inflow in this region.

Infall spectra are notoriously difficult to interpret (Menten et al. 1987), and the change in profile shapes observed in IRS1 require detailed modeling to understand the flows of material in this complex region. Since the clump has a single, central peak and no clear velocity gradient, we use the 1-d radiative transfer code, RATRAN, of Hogerheijde & van der Tak (2000) to model, simultaneously, the dust and line data. The continuum and $H^{13}CO^+$ observations fix the size, temperature, density profile, $H^{13}CO^+$ abundance, mean velocity, and velocity dispersion and tightly constrain the model, leaving only the velocity profile and isotopic ratio as the remaining parameters in the model output HCO^+ line profiles.

The model consists of 10 logarithmically spaced, radially symmetric, shells from $r = 10^{16}$ cm to $r = r_{max} = 10^{18}$ cm (0.32 pc). Ward-Thompson et al. (2000) show that the spectral energy distribution of IRS1 is well fit by the sum of two greybodies consisting of a compact component at 38 K and a larger, cooler component at 17 K that dominates the mass. Based on this, we set the temperature of the outer layer at 17 K and the inner layers, $r < 6 \times 10^{17}$ cm at 38 K. The gas temperature is fixed to be the same as the dust as would be expected at the high densities in the model. Figure 2 shows that the clump is moderately, but not strongly, peaked and we find that the density profile $n_{H_2}(r) = 10^5 (r_{max}/r)^{3/2}$ cm^{-3}, when convolved with a $29''$ beam, matches the dust and velocity integrated $H^{13}CO^+$ maps well. The abundance, $x(H^{13}CO^+) = 2.0 \times 10^{-11}$, systemic velocity, $v = 8.0$ km s^{-1}, and velocity dispersion, $\sigma = 0.8$ km s^{-1}, are set constant in all layers as indicated by the $H^{13}CO^+$ data. The high relative motions between the layers contribute to broaden the output $H^{13}CO^+$ spectra close to the observed 1.0 km s^{-1}. With these parameters, we find that we can reproduce the (radially averaged) continuum fluxes and $H^{13}CO^+$ spectra to within 20%.
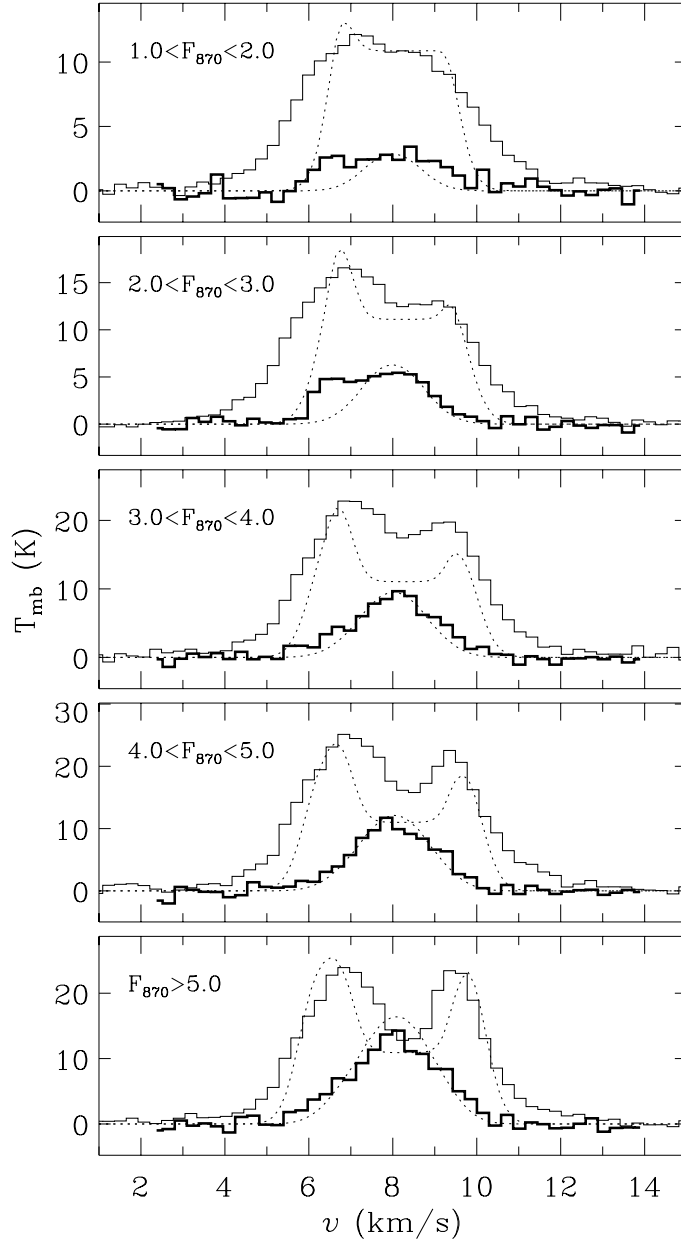
Fig. 4.— HCO$^+$ and H^{13}CO$^+$ 3–2 spectra toward IRS1 (light and heavy lines respectively) averaged over different regions having common dust continuum fluxes, F_{870} Jy. The H^{13}CO$^+$ spectra are shown multiplied by three for clarity. The upper panels are averaged over the outer parts of the core with low continuum fluxes and show large scale infall. The lower panels are averaged over the inner parts of the core with high continuum fluxes and are more symmetric suggesting an overall balance between protostellar outflow and core collapse. The dotted lines show model fits using a spherically symmetric core, constrained by the dust temperature and column density profile and H^{13}CO$^+$ abundance, velocity, and linewidth, that consists of an outer layer collapsing onto an expanding inner region.

Under these constraints, it is not possible to fit the observed HCO$^+$ spectra as closely since only the isotopic abundance and relative velocities between the layers can be varied. Through experimentation with the models, it was found that, given the observed density, temperature, abundance, and velocity profiles, the increasing symmetry of the HCO$^+$ spectra toward the cluster center can only be explained by an outer layer collapsing onto an *expanding* inner region. Figure 4 plots radially averaged model HCO$^+$ and H^{13}CO$^+$ spectra as dotted lines in comparison with the observed data for the case where the isotopic ratio, ^{12}C/^{13}C $= 75$ (implying x(HCO$^+$) $= 1.5 \times 10^{-9}$), and the outer layer ($r = 6 \times 10^{17}$ to 1×10^{18} cm) collapses at a speed $v_{in} = 0.3$ km s^{-1} onto the inner layers ($r = 10^{16}$ cm to 6×10^{17} cm) expanding at a speed $v_{exp} = 1.0$ km s^{-1}.

The combination of large scale collapse and central expansion conspire to match the observed spectral variations from core edge to center because the optical depth is very high in the low density, outer layers and produces a broad (blue and redshifted), self-absorption dip along lines of sight toward the center but only redshifted self-absorption along lines of sight near the edges that do not intercept the inner expanding layer. The velocity of the absorption dip is not observed to change from core center to edge and is reproduced in the model via the increased projection of the radial flow along lines of sight toward the edges. The model spectra have broader self-absorption dips than the data because of the small number of layers in the model and the abrupt change in temperature from 17 K in the outer layer to 38 K in inner layers. Applying a smoother temperature transition and more layers produces more rounded self-absorption dips but at the expense of adding additional parameters to the model.

Because of the radial dependence, $M(< r) \propto r^{3/2}$, most of the mass of the core is in the outer layers and altering the velocities of the innermost layers, $r \lesssim 10^{17}$ cm, does not change the output profiles noticeably. That is, the model resembles the two layer model described by Myers et al. (1996) but with a spherical geometry. With that caveat, the output HCO$^+$ profiles are very sensitive to the optical depth and infall speed of the outer layer and expansion speed of the layer interior to that (which together account for about three quarters of the total mass) and through experimentation with the models we found that the column density and velocities of these layers are constrained to within $\sim 20\%$ by the requirement of matching the observed redshifted absorption at large clump radii and near-symmetry at small radii.

The outer, infalling, layer contains 1/2 the total mass, or about $M_{in} = 400\ M_\odot$, and the mass infall rate onto the cluster is therefore

$$\dot{M}_{in} = M_{in}v_{in}/r_{max} = 4 \times 10^{-4}\ M_\odot \mathrm{yr}^{-1}.$$

This is one to two orders of magnitude greater than infall rates onto solar and intermediate mass protostars (Zhou 1995) as expected for a global infall onto a group of such objects and is similar to the value expected for a gravitational flow, $\dot{M} = \sigma^3/G$, where $\sigma = 1.0$ km s^{-1} is the average velocity dispersion of the core (Figure 3), and G is the gravitational constant (Shu 1977).

The model requires an expanding shell to fit the increasing symmetry toward the core center. Physically, this is probably due to the protostellar outflows in the region, one of which appears to be directed along our line of sight (Schreyer et al. 1997). Shu, Adams, & Liazno (1987) hypothesize that (low mass) stars self-determine their final mass through the removal of a collapsing envelope by their outflows (see also Velusamy & Langer (1998)). By comparing clusters in different evolutionary states and examining the gas flows around them, it will be possible to see if such a process is relevant in a clustered environment where most stars form, and therefore assess its role in the origin of the stellar IMF (Adams & Fatuzzo 1996).

3.2.2. IRS2

Continuum and line emission were lower in IRS2 than in IRS1. The proportion between them, however, was approximately the same and the $H^{13}CO^+$ abundance was found to be consistent with that measured in IRS1, though with a greater uncertainty due to the lower signal-to-noise ratio. Due to the relative weakness of the emission, only the central part of the cluster was mapped in HCO^+ and $H^{13}CO^+$. Figure 5 plots the boundary of the line data on a map of continuum emission. Slight red-shifted self-absorption is found in the average HCO^+ spectrum shown in the left panel. The self-absorption dip is small due to the low optical depth when averaged over the entire mapped region, but is more pronounced in individual spectra, particularly around the dust peaks where the column density is greatest. Both red- and blue-shifted asymmetries are found (see below) but the dominant tendency is for red-shifted asymmetry suggesting, as in IRS1, large scale collapse onto the cluster.

Given the complex resolved structure in IRS2, similar fits to the spectra at different size-scales as in §3.2.1, are not feasible with a 1-d model. However, both simple plane-parallel and spherical two layer model fits to the average spectrum imply an infall speed $v_{in} \simeq 0.3 \pm 0.1$ km s^{-1}. This is similar to the speed of the collapsing layer around IRS1 and implies a similar mass infall rate, $\dot{M}_{in} \simeq 4 \times 10^{-4}$ $M_\odot yr^{-1}$.
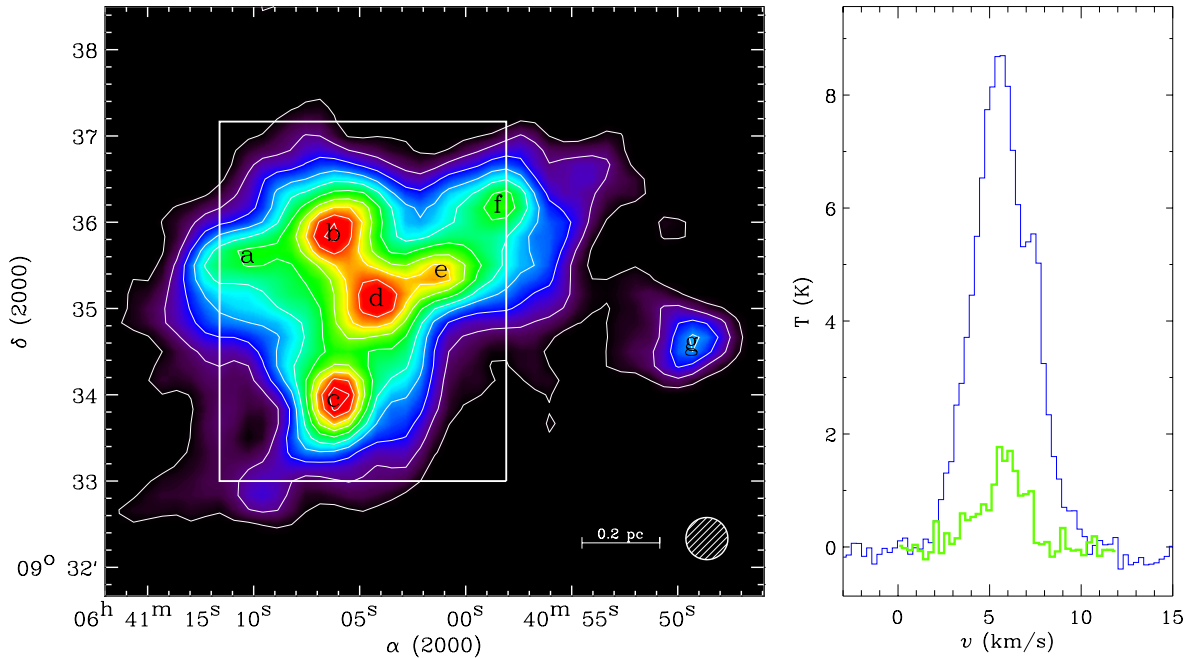

Fig. 5.— Structure and dynamics in the IRS2 cluster. The left panel is a map of the dust continuum emission smoothed to the spectral line resolution of $29''$ as indicated in the lower right corner. Contours begin at and are in steps of 0.2 Jy beam^{-1}. Seven distinct peaks of emission are labeled a-g. The solid dark line marks the boundary of the line data and the white boxes within this outline the different regions over which the average HCO^+ (light lines) and $H^{13}CO^+$ ($\times 3$; heavy lines) spectra in the three left panels, are computed. As with IRS1, the spectra show that large scale inflow is arrested on small scales around protostellar cores.

The greater separation of the protostars in IRS2 allows an investigation of the flows around each one individually. Seven cores, labeled a-g in Figure 5 are apparent as peaks in the dust emission and interpolated

spectra (at a resolution of $29''$) toward the six that lie within the boundary of the line data are shown in Figure 6. A complex mixture of dynamical states are found. Core c has the classic infall profile and core d shows a strong reversed signature. Cores e and f show possible signs of infall and reversed flow respectively but the optical depth is too low to be sure. The HCO^+ spectra toward cores a and b are not readily interpreted in the same manner, due to multiple peaks possibly from absorption by overlapping outflows.

Gaussian fits to the $H^{13}CO^+$ spectra show that the non-thermal velocity dispersion is typically in the range 0.7 to 1.0 km s^{-1} but has a pronounced local minimum of 0.4 km s^{-1} around core b. The resolution of these data is too low to test collapse models in detail but we do not find a correlation between the HCO^+ asymmetry and the $H^{13}CO^+$ dispersion, analogous to that seen in the Serpens cluster (Williams & Myers 2000) and as might be expected from motions driven by the dissipation of turbulence.

To estimate the dynamical influence of each protostar, we have examined average spectra around each one with different smoothing lengths. Although there is confusion from merging at angular scales $\gtrsim 45''$, we find that the overall infall dynamics of the cluster eventually dominate and that the influence of any single protostar does not exceed a radius $60'' \simeq 0.2$ pc.

Core c shows the clearest infall signature with a deep, red-shifted, absorption dip. The infall spectra extend for $\sim 60''$ away from the core before merging with the reversed profiles of spectra associated with core d. The core also has the largest envelope with a total continuum flux of 12.3 Jy and integrated $H^{13}CO^+$ intensity of 2.7 K km s^{-1} within a radius $r = 0.17$ pc, implying a mass $M_{env} = 100\ M_\odot$. The high column density through this envelope is responsible for the deep self-absorption dip, and does not imply a particularly high infall speed. A model fit using the spherically symmetric RATRAN code implies an infall speed $v_{in} = 0.3$ km s^{-1}, and mass infall rate $\dot{M}_{in} = 2 \times 10^{-5}\ M_\odot yr^{-1}$. The speed is the same as the collapse around the entire cluster but the mass infall rate is considerably less because the fit requires only an outer 10 $M_\odot$ layer to be collapsing. Dividing the overall mass infall rate onto the cluster by the number of protostars within it gives an average mass infall rate per protostar about 3 times higher than measured around core c, the one with the clearest individual collapse signature: clearly not all the material falling onto the cluster makes it all the way to the scale of protostars.

The one other core, d, with a deep self-absorption dip shows the opposite asymmetry, indicative of an expanding, rather than infalling, outer layer. It also has the largest $H^{13}CO^+$ linewidth, 1.0 km s^{-1}, in the region. Using a similar model as for core c, the expansion speed is estimated to be 0.5 km s^{-1}. This is likely due to an embedded star although there is no IRAS or MSX point source at its center: higher sensitivity mid-infrared observations are required to determine the stellar content of each core.

Because the envelopes around individual protostars in the cluster are resolved, the optically thin $H^{13}CO^+$ spectra give a measure of the core-core velocity dispersion in the cluster. The six cores, a-f, have a dispersion $\sigma_{c-c} = 0.90$ km s^{-1} and extend over an area with radius $r = 0.44$ pc. Together, these imply a virial mass, $M_{virial} = 3r\sigma_{c-c}^2/G = 250\ M_\odot$. This is less than the total interstellar mass estimated from the continuum observations but is likely much greater than the final stellar mass of the system (Lada et al. 1993). Thus, although the system is currently bound, as the surrounding gas is dispersed through, e.g., stellar outflows, it is likely to become unbound (Lada, Margulis, & Dearborn 1984).

An unbound cluster expands and its age may be estimated from its size and expansion rate. This effect is seen in optically visible clusters in Orion over a range of ages $\sim 3 - 12$ Myr (Blaauw 1991; Brown, Dekker, & de Zeeuw 1997) but the morphology of the two groups IRS1,2 in Figure 1 suggests that it may apply to considerably earlier times. In IRS2, if σ_{c-c} is due to the expansion of the protostellar group, the formation time can be estimated from its crossing time, $t_{cross} = r/\sigma_{c-c} = 5 \times 10^5$ yr, characteristic of late Class I sources
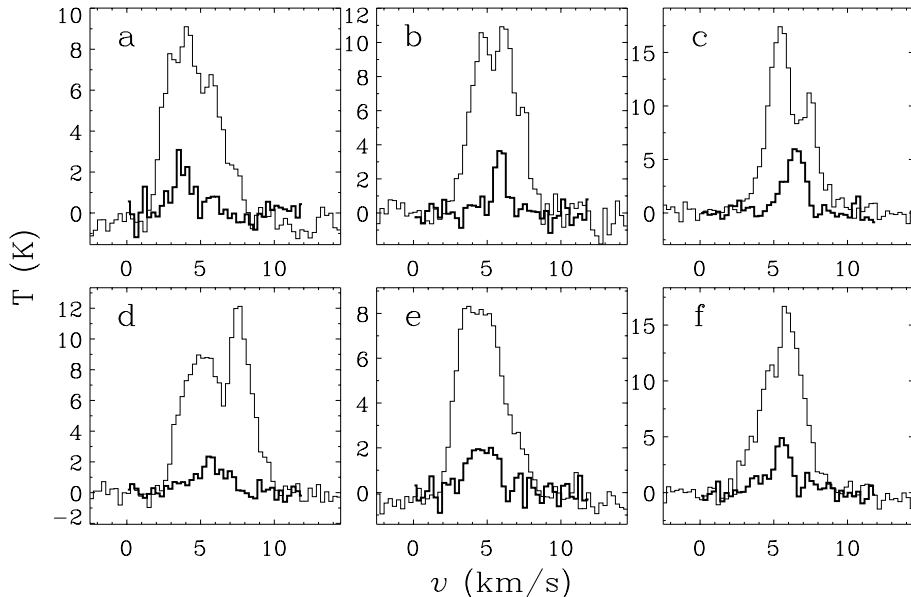
Fig. 6.— HCO$^+$ (light lines) and H^{13}CO$^+$ ($\times$3; heavy lines) spectra toward the individual IRS2 cores a-f as labeled in Figure 5.

(Mundy, Looney, & Welch 2000). The gravitational attraction of the gas around the stellar group should slow their expansion, and the crossing time is therefore an upper limit to the cluster age. Given the continued infall onto the cluster and the large envelope mass, it is not clear if the cluster is actually expanding and whether the crossing time is a useful measure of the cluster age at these early stages in its formation but the suggestive morphology and flux densities of the continuum maps are compelling. Additional observations of other embedded stellar groups in this and other regions will show if there is a consistent pattern. In this regard, we note that a very short integration toward a more extended (and therefore possibly more evolved) group of IRAS sources 11$'$ north of IRS2 did not detect 870 μm emission to an rms flux level of 0.1 Jy beam^{-1}.

4. Conclusion

We have mapped two embedded stellar groups, IRS1 and IRS2, in the NGC2264 region in the continuum at 870 μm and the $J = 3 - 2$ lines of HCO$^+$ and H^{13}CO$^+$. The former shows the thermal emission from the dusty envelopes around the clusters and their protostellar members and the latter show the flows around them; the optically thick HCO$^+$ diagnosing relative motions (infall and outflow) and the optically thin H^{13}CO$^+$ revealing the bulk motion of the clusters and the protostellar velocity dispersion within IRS2.

The two groups have a similar total mass, $M \simeq 10^3 \ M_\odot$, but IRS1 has a much higher peak flux density and is more compact than the more dispersed, lower surface brightness IRS2. In IRS1, comparing the continuum flux density with the integrated line intensity shows that the H^{13}CO$^+$ abundance is constant across the clump at the 29$''$ resolution of these data. Average HCO$^+$ spectra are fit with a radially symmetric model constrained by the dust and H^{13}CO$^+$ data and show a large scale collapse with an infall speed

$v_{in} = 0.3$ km s^{-1} and mass infall rate $\dot{M}_{in} = 4 \times 10^{-4}$ $M_\odot$yr^{-1}, falling onto an inner core expanding at speed $v_{exp} = 1.0$ km s^{-1}. More detailed observations of the competing processes of infall and outflow will show its role in determining stellar masses.

Large scale collapse with a similar infall speed and mass infall rate are found in IRS2 but detailed modeling is precluded by the complex structure that is resolved within. Flows around individual protostars show a mixture of dynamical states ranging from localized collapse with the same speed as the large scale collapse and mass infall rate, $\dot{M}_{in} = 2 \times 10^{-5}$ $M_\odot$yr^{-1}, to expansion at speeds $v_{out} \simeq 0.5$ km s^{-1}. By averaging spectra over increasingly larger size scales, the influence of any one protostar was found to be limited to within a radius $\lesssim 0.2$ pc.

The H^{13}CO$^+$ spectra in IRS2 was used to measure the protostellar velocity dispersion and thereby infer the virial mass of the system. This was found to be less than the total mass enveloping the cluster but more than the stellar mass indicating that the group is destined to become unbound as the surrounding gas and dust are dispersed by protostellar winds and outflows. The expansion of an unbound stellar group may already have started in IRS2 where the greater separation of individual protostars and the low column density toward them, relative to IRS1, both suggest a more evolved system. In this case, an upper limit to its age, $\sim 5 \times 10^5$ yr, can be determined kinematically by assuming a constant expansion speed equal to the observed protostellar velocity dispersion. Additional observations of other clusters are necessary to see if there is a pattern between cluster sizes, velocity dispersion, and evolutionary state, but this technique – a well known tool for optical clusters – may be a useful new approach for following protocluster and protostellar evolution.

The dominant mode of stellar birth is in groups and these observations provide new insight into their formation. To examine cluster formation at earlier times will require higher resolution observations of dense, compact cores such as IRS1, while large scale, high sensitivity imaging of the dust and gas around more evolved systems than IRS2 can follow the evolution at later times than discussed here.

REFERENCES

Adams, F.C. 2000, ApJ, 542, 964

Adams, F.C., & Fatuzzo, M. 1996, ApJ, 464, 256

Allen, D. A. 1972, ApJ, 172, L55

Bergin, E.A., Ungerechts, H., Goldsmith, P. F., Snell, R. L., Irvine, W. M., & Schloerb, F. P. 1997, ApJ, 482, 267

Blaauw, A. 1991, in *The Physics of Star Formation and Early Stellar Evolution*, eds. C.J. Lada & N.D. Kylafis

Brown, A. G. A., Dekker, G., & de Zeeuw, P. T. 1997, MNRAS, 285, 479

Hogerheijde, M. R., & van der Tak, F. F. S. 2000, A&A, 362, 697

Lada, C. J., Margulis, M., & Dearborn, D. 1984, ApJ, 285, 141

Lada, C. J., Young, E. T., & Greene, T. P. 1993, ApJ, 408, 471

Lada, C. J., Lada, E. A., Clemens, D. P., & Bally, J. 1994, ApJ, 429, 694

Leung, C. M., & Brown, R. B. 1977, ApJ, 214, L73

Margulis, M., Lada, C. J., & Snell, R. L. 1988, ApJ, 333, 316

Margulis, M., Lada, C. J., & Young, E. T. 1989, ApJ, 345, 906

Menten, K. M., Serabyn, E., Guesten, R., & Wilson, T. L. 1987, A&A, 177, L57

Mundy, L.G., Looney, L.W., & Welch, W.J. 2000, in *Protostars and Planets IV*, eds. V. Mannings, A.P. Boss & S.S. Russell, 355

Myers, P. C., Mardones, D., Tafalla, M., Williams, J. P., & Wilner, D. J. 1996, ApJ, 465, L133

Oliver, R. J., Masheder, M. R. W., & Thaddeus, P. 1996, A&A, 315, 578

Rohlfs, K., & Wilson, T. L. 1996, *Tools of Radio Astronomy* (Heidelburg: Springer)

Sargent, A. I., van Duinen, R. J., Nordh, H. L., Fridlund, C. V. M., Aalders, J. W., & Beintema, D. 1984, A&A, 135, 377

Shu, F. H. 1977, ApJ, 214, 488

Shu, F. H., Adams, F. C., & Lizano, S. 1987, ARA&A, 25, 23

Sung, H., Bessell, M. S., & Lee, S. W. 1997, AJ, 114, 2644

Schreyer, K., Helmich, F. P., van Dishoeck, E. F., & Henning, Th. 1997, A&A, 326, 347

Thompson, R. I., Corbin, M. R., Young, E., & Schneider, G. 1998, ApJ, 492, L177

Ungerechts, H., Bergin, E. A., Goldsmith, P. F., Irvine, W. M., Schloerb, F. P., & Snell, R. L., 1997, ApJ, 482, 245

Velusamy, T., & Langer, W. D. 1998, Nature, 392, 685

Walker, C. K., Lada, C. J., Young, E. T., Maloney, P. R., & Wilking, B. A. 1986, ApJ, 309, L47

Ward-Thompson, D., Zylka, R., Mezger, P. G., & Sievers, A. W. 2000, A&A, 344, 1122

Williams, J. P., & Myers, P. C. 1999, ApJ, 511, 208

Williams, J. P., Myers, P. C., Wilner, D. J., & Di Francesco, J. 1999, ApJ, 513, L61

Williams, J. P., & Myers, P. C. 2000, ApJ, 537, 891

Wolf-Chase, G. A., & Gregersen, E. 1997, ApJ, 479, L67

Wolf-Chase, G. A., Walker, C. K., & Lada, C. J. 1995, ApJ, 442, 197

Zhou, S. 1995, ApJ, 442, 685